



NASA Public Access

Author manuscript

IEEE J Sel Top Appl Earth Obs Remote Sens. Author manuscript; available in PMC 2019 February 01.

Published in final edited form as:

IEEE J Sel Top Appl Earth Obs Remote Sens. 2018 February ; 11(2): 498–512. doi:10.1109/JSTARS.2017.2784784.

Mapping Double and Single Crop Paddy Rice With Sentinel-1A at Varying Spatial Scales and Polarizations in Hanoi, Vietnam

Kristofer Lasko,

Department of Geographical Sciences, University of Maryland, College Park, MD 20740 USA

Krishna Prasad Vadrevu,

Earth Science Office, NASA Marshall Space Flight Center, Huntsville, AL 35805 USA

Vinh Tuan Tran, and

Faculty of Information Technology, Hanoi Pedagogical University 2, Hanoi, Vietnam

Christopher Justice

Department of Geographical Sciences, University of Maryland, College Park, MD 20740 USA

Abstract

Paddy Rice is the prevalent land cover in the mosaicked landscape of the Hanoi Capital Region, Vietnam. In this study, we map double and single crop rice in Hanoi using a random forest algorithm and a time-series of Sentinel-1 SAR imagery at 10 and 20 m resolution using VV-only, VH-only, and both polarizations. We compare spatial and areal variation and quantify input band importance, estimate crop growth stages, estimate rice field/collective metrics using Fragstats with image segmentation, and highlight the importance of the results for land use and land cover. Results suggest double crop rice ranged from 208 000 to 220 000 ha with 20-m resolution imagery accounting for the most area in all polarizations. Based on accuracy assessment, we found 10 m data for VV/VH to have highest overall accuracy (93.5%, $\pm 1.33\%$), while VV at 10 and 20 m had lowest overall accuracies (90.9%, ± 1.57 ; 91.0%, ± 2.75). Mean decrease in accuracy suggests for all but VV at 10 m, data from harvest and flooding stages are most critical for classification. Results suggest 20 m data for both VV and VH overestimates rice land cover, however 20 m data may be indicative of rice land use. Analysis of growing season suggests average estimated length of 93–104 days for each season. Commune-level results suggest up to 20% coefficient of variation between VV10m and VH10m with significant spatial variation in rice area. Landscape metrics show rice fields are typically planted in groups of 3–4 fields with over 796 000 collectives and 2.69 million fields estimated in the study area.

Personal use is permitted, but republication/redistribution requires IEEE permission. See http://www.ieee.org/publications_standards/publications/rights/index.html for more information.

This work was supported by the University of Maryland, Council on the Environment Green Fund Fellowship and American Society for Engineering Education SMART scholarship. The work of K. Lasko was supported in part by the Science, Mathematics, and Research for Transformation scholarship by the American Society for Engineering Education. (*Corresponding author: Kristofer Lasko.*)

klasko@umd.edu, krishna.p.vadrevu@nasa.gov, trantuanvinh@hpu2.edu.vn, cjustice@umd.edu

Keywords

Agriculture; image classification; land cover; radar applications; red river delta; rice; spatial analysis; Vietnam

I. INTRODUCTION

RICE (*Oryza sativa*) is the staple crop for economic and cultural livelihood throughout much of Southeast Asia, including Vietnam. Production of paddy rice in Vietnam has been expanding consistently over time with 32.5 million metric tons produced in year 2000 to 45.2 million metric tons in the year 2015 [1]. All the while, area under cultivation has only slightly increased with 7.67 million ha in 2000 and 7.83 million ha in 2015, suggesting notable agricultural intensification. Intensification is critical especially in areas of the Red River Delta such as the Hanoi Capital Region, where population pressure and a robust economy are driving periurban expansion into agricultural areas [2]. Thus, reducing the amount of area under cultivation in some areas.

Accordingly, it is of increasing importance to develop efficient methods for mapping paddy rice in Vietnam. The two dominant rice-producing hubs in Vietnam are within the Red River Delta and the Mekong River Delta, together accounting for the majority of national rice production. Optical imagery such as from MODIS or Landsat are frequently cloud contaminated during key agricultural stages (i.e., planting and harvest); thus, hampering mapping efforts [3]. C-band Sentinel-1 imagery is capable of penetrating through cloud cover making it the obvious choice for timely mapping of paddy rice.

Efforts to map paddy rice using SAR originated in the 1990s with selected images from ERS-1 C-band imagery with approximately 12.5–30 m spatial resolution and a repeat pass of 35 days [4]–[9], and also using C-band RADARSAT at spatial resolution of 10–100 m and a repeat pass of 24 days [10]–[12]. These pioneering studies were often stymied by lack of quality ground-truth imagery, single polarization, or were limited to small spatial scale studies due to high data volumes. Subsequent studies began focusing on utilizing multitemporal SAR over larger land areas for improved rice mapping and testing various algorithms with ERS-1, ERS-2, and RADARSAT [13]–[17]. Improvements in sensors and availability of ground-truth data led to further more extensive rice mapping studies using L-band SAR such as ALOS/PALSAR or JERS-1 [18], [19], ENVISAT ASAR [20]–[23], TerraSAR-X and COSMO-SkyMed [24]–[27]. Recent studies include RADARSAT-2 data, object-oriented crop mapping [28], [29], combined optical and SAR data [30]–[32], and Sentinel-1 C-band SAR [33]–[35]. More details are available in a recent review [36].

While a variety of strong classification methods exist, a number of recent studies have employed random forests for SAR applications, including wetlands mapping [37]–[39], general agriculture/land cover [40], and in paddy rice mapping with promising results [41]–[43]. Recent remote sensing studies have also included use of texture-based classification such as Gray Level Co-occurrence Matrix (GLCM) with promising results [22], [44], [45]. In addition to mapping paddy rice areal extent, other studies have employed SAR for agricultural phenology estimation with multitemporal imagery [46], [47], including studies

with rice paddy fields and polarization variation, [48]–[55]. While some of these studies applied time-series filters to derive accurate phenology metrics, these are not always requisite due to the unique dynamic range of paddy rice signal from SAR [41]. The SAR signal seen in a time-series can accurately capture different stages of crop growth useful for monitoring biophysical variables as well as length of season, planting, and harvest dates. While local farmers and stakeholders have knowledge of the crop phenology, SAR-based information is useful for broader national or regional operational monitoring of crops (i.e., crop conditions, status, or health) which is a major goal of international initiatives such as Asia-Rice Crop Estimation and monitoring (Asia-RiCE) project or the Global Agricultural Monitoring (GEOGLAM) initiative [56], [57]. The SAR observations can survey the entire region, whereas optical data can often be obstructed by cloud. Thus, SAR data can be useful for crop mapping and monitoring at regular intervals.

II. STUDY AREA AND DATASETS

A. Study Area

The mosaic landscape of the Hanoi Capital Region includes a variety of land cover types dominated by rice agriculture, as well as other small-holder croplands, urban areas, small plantations, and aquaculture. The typical rice field size in the area is about 800 m² with fields routinely planted in large collectives as necessary to facilitate irrigation. The field size is suitable for moderate-to-fine resolution mapping [58]. The Hanoi Capital Region is situated within the Red River Delta, Vietnam's oldest rice producing region, accounting for about 15% of the country's total rice production [1]. Of all the different crops, rice is most prevalent and it is the dominant crop type in the region. It has two distinct seasons: Winter-Spring, and Spring-Summer. Rice has three distinct stages: sowing/transplanting, growth, and harvest/post-harvest, all of which can be identified using satellite data [8]. In the study area, rice is sown or transplanted after the Tet holiday in February or early March. Subsequently, a significant green-up is observed as the rice matures in its vegetative stage, especially after heading in April [59], [60]. During late May to June the rice is harvested, and rapidly prepared for the next season starting in late June or July. After the harvest in each season (June and October) the rice residues including straw and stubble, are regularly burned accounting for as much as 13% of PM_{2.5} emissions for Vietnam; thus, burning may constitute a significant air quality issue [58], [61].

The rice fields are supported by a vast network of irrigation and drainage canals and small access roads seen throughout the region. While most fields practice double cropping, some fields cultivate a single crop of rice. After the harvest, single rice fields remain flooded to support the growing aquaculture industry [62], [63]. The study area has seen rapid expansion of aquaculture with 16.50000 ha in year 2000, and 46 000 ha in year 2014, with the vast majority of growth occurring in Hanoi province [1].

1) Satellite Data: The Sentinel-1 satellite from the European Space Agency provides C-band SAR imagery (5.4 GHz) near globally with a 12 day revisit time or 6 day revisit time depending on availability of Sentinel-1B imagery. The Sentinel-1 imagery is provided as dual-polarized Interferometric Wide swath (IW) data with vertical transmit, vertical receive

(VV), and vertical transmit, horizontal receive (VH) polarizations. Each polarization is at a nominal spatial resolution of $5\text{ m} \times 20\text{ m}$ prior to preprocessing using an open-access operational baseline observation strategy. A full time-series stack of 22 Sentinel-1A images was acquired during the 2016 growing season (February–October) (see Table I). No Sentinel-1B imagery was available over the study area. Level-1 ground-range detected, descending mode, IW imagery acquired from the Alaska Satellite Facility (a direct mirror of ESA’s Sci-hub) were processed using the free and open source Sentinel-1 toolbox. The ground-range detected images were processed following guidelines including applying restituted orbit files, multilook azimuthal compressions to 20 m, terrain correction using SRTM30m version 4DEM, radiometric calibration adjustments to correct for viewing geometry effects, and refined lee speckle filter to reduce constructive and destructive interference, all resulting in sigma-nought backscatter data logarithmically scaled in decibel [64]. Given the relatively small study region with generally flat terrain, incident angle artifacts and layover/shadow effects were relatively minimal. We display incident angle and SAR backscatter ranges across the study area in Table I. We also highlight average SAR signal and the temporal dynamic across the different land cover types found in the study area (see Fig. 1).

2) Training and Validation Data: We conducted fieldwork throughout the study area during May/June and September/October of 2016 as part of a related project on rice residue burning. The data included surveys on crop calendar, crop rotation, field conditions, and biomass data. Over 900 geolocated photos were taken of paddy fields and nonrice areas such as aquaculture, wetlands, and other land cover types found within the region. These field photos were used for training or validation along with fine-resolution imagery from Google Earth and the original Sentinel-1 imagery. No training data were included in the validation. We show a multitemporal composite of the SAR data with the training polygons overlaid (see Fig. 2).

III. METHODOLOGY

We classified the six different datasets (see Table II) using the random forest algorithm to obtain rice areal estimates and as a basis to compare the datasets. These resulting datasets were the basis for comparison of the different polarizations and spatial resolutions for mapping small-holder paddy rice. Accordingly, we selected nominal 10-m resolution as it is the native resolution of Sentinel-1 and 20-m resolution data for comparison. We addressed the following questions in our study: 1) Which dataset yields the highest overall and class specific accuracies and mapped areas, and are there notable differences between them? 2) What is the typical rice phenology including start/end of season and length of growing season? 3) How do the resulting mapped rice area estimates vary at the province and commune level? 4) Based on landscape analysis, what are the spatial characteristics of paddy fields and approximately how many are in the study area?

A. Double and Single Crop Rice Mapping

We employed an ensemble, machine-learning random forest algorithm for mapping single and double crop paddy rice, as well as for evaluating the relative importance of specific

input data for mapping [65]. The machine-learning random forest algorithm implemented in Scikit-learn python package uses bootstrap aggregated sampling to build individual decision trees for classification. Each decision tree was built with a bootstrap sample from the training data, with the unsampled data used for out-of-bag sampling. Within the structure of a tree, a random sample of the square root of the number of predictors was chosen for each split as best candidates derived from the entire predictor set. Random forest is robust against outliers and overfitting, nonparametric, has high classification accuracy, and can yield a measure of variable importance.

We implemented the random forest algorithm using all 22 (VV or VH) or 44 input bands (VV & VH) (see Table I) for each of the six datasets separately. We populated the random forest with 1000 trees, where out-of-bag errors reach asymptotic values [65]. The same classification technique was applied to each dataset. Out of bag samples, which are randomly withheld from classification training were used as an indicator of feature importance. From the 1000 trees populated in our random forest, the mean decrease in classification accuracy for the input bands was reported. This was useful as a measure of feature importance in mapping paddy rice and each input band can be linked to a general crop growth stage (i.e., sowing, vegetative growth, and harvest). Training polygons were digitized over the single rice, double rice, and nonrice areas within each province using field photos, Sentinel-1 data, survey information, and fine-resolution Google Earth imagery.

B. Accuracy Assessment

We performed an accuracy assessment on the resulting rice maps. Random points across the study area were generated using a stratified random sampling scheme [66]. Based on the proportion of each resulting mapped class, a stratified random sample of 402 total polygons for double crop rice (125), single crop rice (41), and nonrice (236) classes were generated for the 10 m data. For the 20 m data, the same polygons were used for comparison consistency; however, there are fewer total pixels due to reduced spatial resolution. We specified a 600 m minimum distance between polygons to prevent field overlap.

Following good practices in accuracy assessment, we adjusted the classification accuracies as well as the mapped rice area estimates based on the weighting from the proportion of land area for each class [67]. This weighting results in unbiased areal estimates. Based on the same, we derived uncertainty estimates for the accuracy-adjusted areas using a 95% confidence interval for each of our resulting mapped classes. The accuracy-adjusted area provides a more robust assessment of the area mapped for each class. We also computed the confidence intervals for adjusted class and overall accuracies to be used for comparison among the different maps.

C. Spatial Analysis

We compared the paddy rice maps through a number of metrics including average absolute deviation (AAD) (1) and coefficient of variation (CV) (2) to explore absolute and relative variation in mapped area for each of the six different datasets as follows:

$$AAD = \frac{\sum |x - \bar{x}|}{N} \quad (1)$$

$$CV = \left(\frac{\sigma}{\bar{x}}\right)100 \quad (2)$$

where x is the rice area in hectares for one of the six rice maps, \bar{x} is the mean rice area of all six datasets, and N is the number of datasets for (1), while for (2) σ is the standard deviation of all rice area for all six datasets, and \bar{x} is the mean rice area for all datasets. The final value is a percentage.

We compared the AAD and CV at the commune-level (third-level administrative subdivision) and study-area level to assess overall and spatial variability. In addition, we computed pixel-level thematic change for each dataset. We also employed Fragstats (Version 4.2) for landscape-scale analysis on the most accurate resulting dataset including number of patches (collections of connected/adjacent paddy rice pixels) and patch metrics useful for evaluating the size of large connected aggregations/collections of paddy rice fields. Further, we employed mean-shift image segmentation on the double-rice pixels of the time-series imagery stack to estimate rice collective size (groups of fields with similar crop phenology) and number of fields in the study area by including typical paddy field size of 790 m² [58]. We show the general flowchart in Fig. 3. Meanshift image segmentation is a nonparametric iterative algorithm fitting a neighborhood window around each pixel, calculating the data mean in the window, and shifting the neighborhood window to the mean [68], [69]. The algorithm is useful for clustering pixels with similar signal and has been used in a variety of land cover remote sensing applications [70], [71].

D. Rice Phenology

While some of the prior studies utilized spatiotemporal filtering to derive crop phenology metrics, we derived the metrics based on the unique rice dynamic range combined with general phenology time frames. Sentinel-1 VH-polarized backscatter imagery were used to estimate sowing /transplanting and harvest dates for both seasons of rice. Based on the unique phenology of paddy rice measured by SAR and selecting a general timeframe based on a *priori* knowledge, we found local planting date coincides with the local minimum value (indicative of flooding, constrained to February or March), and harvest date when the local maximum backscatter value is reached (indicative of peak maturity of rice just prior to harvest, constrained to May or June) as noted in previous studies [8], [41], [48], [72]. The estimated range is based on the overpass dates of the Sentinel-1 satellite. The approximate length of growing season is derived by differencing the median date within the planting range and the harvest date range.

IV. RESULTS

A. Mapped Area Variation

The six paddy rice maps generated from the random forest classifier and their spatial patterns are shown in Fig. 4. The pixel classification count for double rice shown in Fig. 4 zoomed to a hotspot of variation area in Bac Ninh, highlights that along edges and smaller fields some of the rice maps are not in agreement. Overall, 66% of the pixels were in agreement (where pixel count = 6). On another note, when the absolute mapped rice areas are compared, we notice more variation. For example, the total mapped double-rice area for each is: 208 276 ha (VV-10m), 212 465 ha (VH-10m), 214 565 ha (VV&VH-10m), 214 903 ha (VV-20m), 218 788 ha (VH-20m) and 220 356 ha (VV&VH-20m). This general pattern suggests 10 m imagery, systematically reports lower mapped area than 20 m imagery, and VV reports less mapped area than VH with VV&VH combination accounting for the most area. This is attributed to VV signal attenuated by the vertical structure of rice. The same pattern is not clear for single rice. Whereas 10 m datasets exhibited less area than 20 m datasets, and reported areas varied between polarizations. In comparison to the official government rice areal statistics for 2016 of 232 700 ha paddy rice, our estimates reported about 12 000–24 000 ha less [1]. In comparison to same statistics for the entire Red River Delta (546 950 ha), our study area has about 40% of the total rice area. The mapped areas for single rice can be seen in Table III.

B. Accuracy Assessment and Areal Adjustment

We evaluated the accuracy of each dataset and present the confusion matrices with the total number of pixels for each class, as well as user, producer, and overall accuracies adjusted using the unbiased areal estimates. We also provide 95% confidence intervals for each statistic for purposes of comparison. The dataset overall accuracies in descending order are VV&VH-10m (93.5%), VH-10m (93.1%), VV&VH-20m (92.5%), VH-20m (91.4%), followed by VV-20m (91.0%), and VV-10m (90.9%). We note the confidence interval ranges between VV&VH20m and VV&VH-10m, and the same for the others, suggests they may not be significantly different overall. However, when comparing class specific user and producer accuracies for double crop rice and single crop rice the differences are clear. The biggest difference is for single crop rice where the 10 m datasets have higher user and producer accuracies (except VV). For double crop rice, the user and producer accuracies are higher in the 10 m than the 20 m datasets. Across all datasets, user accuracies for single and double crop rice are higher than producer accuracies suggesting a net-positive of rice omission errors. Further details on the confusion matrices are shown in Table III.

We adjusted the total mapped areas based on the accuracy assessment and resulting unbiased areal estimates for each dataset and compared the trends as shown in Fig. 5. Overall, we found that accuracy-adjusted areas for single and double rice were higher than the mapped areas. This is due to the rice omission errors found during the accuracy assessment. The accuracy adjusted areas yield an improved areal estimate useful for studies requiring rice land area as a nonspatial input. The 95% confidence intervals for each class are also shown in Fig. 5 highlighting uncertainty in the mapped areas.

C. Land Cover and Land Use

We visually compared the six different datasets with fine resolution Google Earth imagery. We highlight one location representative of the pattern throughout the study area (see Fig. 6). While all datasets capture the general rice spatial patterns well, there are some errors and variation. Specifically, the VH10m and VVVH-10m datasets are best able to reduce commission errors from small irrigation ditches and roads adjacent or within rice fields. All 20 m datasets do not effectively account for these areas regardless of polarization due to spatial resolution. While it is technically error, we highlight that this rice area commission error could be useful for certain applications seeking to map not only rice land cover, but also mapping rice land use. While these ditches and roads are not rice, they are designed to support rice field operations (threshing or drying of rice occurs in these areas) and access to fields (such as for machine-harvester equipment). However, while the 20 m datasets are including these adjacent roads or ditches in the rice category through commission errors, they have fewer false small rice areas (seen as small 5 or 6 pixel collections on the eastern sides of the imagery). One reason for this is attributed to inherent noise reduction through data processing involving multilook processing into 20 m resolution. Thus, there are tradeoffs to each resolution and polarization.

D. Pixel-Level Rice Variation

Analysis of pixel-level thematic variation between each dataset was conducted. For the 10 m datasets, we found the biggest difference between VV and VH where 48 372 ha of classified land area were different (6.29% difference) which is much higher than total rice area variation (214 565 ha VH10m vs 208 276ha VV10m). The main differences were attributed to double-rice pixels converted to nonrice pixels, nonrice converted to double rice, followed by nonrice into single rice. The smallest difference was between VH and VV&VH with 12 343 ha (1.60% difference). In descending order, the majority was attributed to nonrice to double rice, double rice to nonrice, and nonrice to single rice. The 20 m datasets change was very similar with VV and VH (46 613 ha with 6.01% difference), VV and VV&VH (39 848 ha with 5.18% difference), and VH and VV&VH (10 288 ha with 1.34% difference). In all cases, 20 m datasets had about 0.2% less difference than the 10 m datasets, with each following a similar pattern of variation.

E. Province-Level Rice Variation

We evaluated the province-level variation in mapped rice area between the different datasets through CV and z-scores for double and single rice (see Fig. 7). The CV results suggest relatively low and uniform variation in double rice across the provinces with highest variation in Bac Ninh (2.82%) and Hanoi (2.30%) followed by Ha Nam (2.02%), Vinh Phuc (1.92%), and Hung Yen (1.77%). For single rice, the variation was wide ranging depending on the province, with Vinh Phuc exhibiting the highest (11.57%) variation followed by Bac Ninh (8.90%), Hanoi (8.37%), Ha Nam (5.71%), and Hung Yen (4.17%). We attribute the highest variation in Vinh Phuc to small-holder agriculture and mosaicked landscape making classification difficult. The z-score results for double-rice suggested more insight into province-level variation. For VV20m Ha, Nam and Hung Yen had the highest positive z-scores whereas all other provinces had negative Z-scores, and that VV had the most variation

in z-score across the provinces. This suggests the VV may be more sensitive to different environmental parameters such as water and moist soil underlying much of these areas. We note similar Z-scores for VVVH20m with the least variation across provinces in single and double crop rice. The same also goes for VH20m with all z-scores for each dataset as positive. Generally, the 20 m datasets tend to have more similar z-scores than the 10 m datasets.

F. Commune-Level Rice Variation

For the entire study area, the total mapped double rice area for each dataset is relatively similar ranging from: 208 276ha (VV10m) to 220 536ha (VVVH20m). However, results at the commune level (third-level administrative subdivision) suggest more variation. We note that while VV10m had the overall lowest double-rice mapped area, the trend is not spatially universal as VV10m had 27 communes with more rice than VH10m. For example, VH10m in Loung Tai had 249ha less rice than VV10m with a percent difference of 4.60%. However, the biggest percent difference between the two was in Ba Vi, where VV10m had 20% less rice than VH10m.

To better evaluate spatial variation at the commune level, we measured the AAD and CV. Across all communes for each dataset, we found rice area did not vary uniformly across space, based on the AAD and CV results (see Fig. 8). We found an average CV of 4.75% for each commune. The spatial pattern suggested that much of the variation proportionately occurred in the northern half of the study area (Vinh Phuc, northern Hanoi, and northern Bac Ninh provinces), whereas communes in Hung Yen and Ha Nam had variation between the datasets almost always less than 2.5%. We also note that the communes surrounding Hanoi City had relatively higher CV, but low AAD due to small amount of rice in these areas. We attribute the spatial clustering of variation to land cover and land use differences, and the difficulty of mapping in a small-holder mosaicked landscape. Accordingly, the northern areas dominated by more wetlands, hills, and especially smaller rice fields intermixed with smallholder nonrice crops are likely to have greater class confusion.

G. Rice Phenology

We estimated the length of growing season, start of season, and end of season for rice based on the SAR time-series and area difficulties in more mosaicked landscapes with smaller fields. The unique dynamic range in SAR signal found for rice paddies (see Fig. 9). The results were aggregated to commune level for comparison. Across all communes, we found an average length of the first rice season to be 93 days, while the second season was approximately 104 days. We attribute the relatively lower range in season 1 due to most fields remaining flooded for several months from the previous season harvest and missing SAR data for ~June 28th. In reality, the first season length is likely slightly underestimated. In addition, these are approximations dependent on the Sentinel-1 overpass dates (± 11 days). The estimated average sowing date for the second season is Day of Year (DoY) 175 (23rd of June) and DoY 55 (24th of February) for the first season. For the harvest, we found an average DoY of 148 (27th of May) for season 1, whereas for season 2 we found estimated average harvest of DoY 279 (5th of October). These estimates are generally in line with our local knowledge and field experience. A more precise estimate of length of season, harvest,

and sowing could be obtained by including both Sentinel-1A and Sentinel-1B, cutting the overpass time in half.

H. Rice Landscape Metrics

Fragstats analysis using the most accurate VVVH10m map produced a total of 31 934 large continuous tracts/patches of double-rice pixels with an average area of 6.72 ha ($\sigma = 59.4\text{ha}$) and large standard deviation. Mean-shift image segmentation combined with fragstats analysis on the time-series stack masked for double-rice pixels, suggests 796 720 rice collectives (small patches of rice with similar SAR signal) with an average area of 2668m² ($\sigma = 7250\text{m}^2$). The average field size is reported to be 790m² ($\sigma = 625\text{m}^2$) [58]; thus, an average of 3.4 individual rice fields make up a typical rice collective which follow a similar rice phenology pattern including harvest and flooding dates, due to similarity in image segmentation. Based on the aforementioned average field size and total double-rice area from the VVVH10m scenario, we estimate 2.69 million double-rice paddy fields within the HCR.

I. Input Band Importance

The feature importance of each input band for the paddy rice classification was assessed in the random forest classifier through mean decrease in accuracy (see Fig. 10). We found that the top 3 most important bands for VH(10 m and 20 m), and VV(20 m) were generally the same with bands 11, 12, and 13 (see Fig. 10). These three bands were from June and early July (see Table I) suggesting that imagery from spring harvest and summer planting season are most important as removing one of these bands results in a mean decrease in accuracy of 3–6% depending on the dataset. In addition, these bands are important for discriminating between single and double crop rice. Other bands obtained during planting, growth, and harvest, however, are also important as removing any one of them still reduces overall accuracy significantly. For VV (10 m only), we found bands 7, 6, and 8 to be most important. These bands are from the main vegetative growth stage for winter rice (April). A relatively similar trend was observed in VVVH datasets. The average local incidence angle and standard deviation over rice areas suggests minimal variation in incidence angle ($\mu = 38.63^\circ$, $\sigma = 3.34^\circ$). Thus, it is not critical to account for the incidence angle variation effects on backscatter in the study area (see Table I) due to minimal variation. In addition, the time-series signal of double rice versus single rice shows it is possible to differentiate between the two with only the first season of data. Double rice areas have relatively higher backscatter throughout the first rice season (see Fig. 1).

V. DISCUSSION

Early rice mapping studies in Asia employing SAR have had varying degrees of success and accuracy. Some of the earliest studies using RADARSAT or ERS-1 found good agreement between their rice maps and existing validation data, with the latter study reporting overall accuracy of 87% for a small study area and coarse resolution imagery [5], [8], [11]. More recent studies employing C-band RADARSAT imagery have reported rice class accuracies as high as 98% and 90% using TerraSAR-X imagery [30], [72]. Studies have also highlighted advantage of multirate versus single-date imagery for rice mapping [28].

However, in Vietnam the case is different. In the Mekong River Delta using multitemporal SAR including ENVISAT and Sentinel-1, studies have found overall accuracy for land cover or rice maps ranging from 80–92% [20], [21], [23], [31], [33], [35] [73]. In the Red River Delta, using multitemporal SAR such as RADARSAT-2 and ENVISAT, studies have found overall accuracy for rice maps ranging from 71–95% [29], [41], [74], [75]; and overall accuracy of 89% in Vietnam with TerraSAR-X [27].

Our accuracy assessment found overall strong user's accuracies for most datasets and classes with double rice ranging from 92.1–96.9% and single rice (95.2–100%), whereas, producer's accuracies were generally lower (77.8–83.5% double rice, and 35.0–59.0% single rice) with overall accuracies between 90.9–93.5%.

Our study findings are important in that the different spatial resolution or polarization combinations have significant impacts on mapped rice area. While these differences may not be high at the study area scale, the difference between the datasets is high at the commune and pixel level with CV averaging about 10% at the commune scale. The most variation was found in communes in the northern half of the study area in Northern Hanoi, Vinh Phuc, and Bac Ninh where small-holder farms in mosaicked landscapes are dominant, making mapping difficult [2], [74]. These spatial differences are important for different rice mapping applications where spatial location is critical, such as rice straw burning emissions and air quality assessments. We highlight the importance of selecting the most accurate map which in this case is VVVH10m. We also demonstrate through comparison at different spatial scales that 10 m data have more variation in rice area compared to 20 m data. We find that 20 m data may prove effective for land use mapping due to inclusion of a variety of classes such as irrigation canals, and adjacent dirt farm roads, whereas 10 m may be best for specific thematic (rice in our case) mapping. Our study also found that VH polarization were more accurate than VV polarizations for rice mapping. This has been attributed to VV more influenced by standing water in fields and the signal attenuated by vertical structure of rice [21], [35], whereas VH is less affected and more representative of the actual rice growth and plant canopy structure [33]. We also found our map had slightly more rice area than the official government data, and other rice mapping studies have found good agreement between maps and government data in Vietnam [60], [74].

Using a simple method to replicate metrics on rice phenology, we demonstrate the utility of our phenology estimates for regional and global rice monitoring systems such as Asia-RiCE or GEOGLAM. Additional applications could improve upon existing SAR and MODIS disaster management strategies with improved phenology metrics [76]. This is also demonstrated through random forest feature importance metrics that reducing some input data (i.e., near harvest) can yield slightly less accurate maps as they may not capture the wide backscatter range useful to distinguish paddy rice from other land cover classes. However, these maps are still useful for operational monitoring applications.

Combining our most accurate rice map with image segmentation, Fragstats landscape analysis and field data, we estimated the total number of paddy rice fields in the study area (2.69 million). In addition, we found the average size of continuous rice area patches, as well as the estimate of the average size of a rice collective (2668m², or 3.4 rice fields). As

mentioned, the rice collectives are continuous rice areas undergoing similar rice phenology (i.e., managed in-sync).

While other classification methods could have been used, we chose random forest as it is robust, widely applied, generally has similar results in agricultural applications [43], is less of a black box, and computes faster than other algorithms such as support vector machines or artificial neural networks [77]. Ensemble mean classifiers such as random forest also outperform standard approaches such as single decision tree or maximum-likelihood classifier [42]. Random forest classifier is also used for reducing feature inputs to reduce data dimensionality, processing time, and redundancy [78],[79], whereas for this study, we maintained all inputs as we already needed the full time-series of SAR for growing season estimates.

Our study was limited due to several factors. The availability of Sentinel-1A, but not 1B, limits data input to approximately 12 day time intervals. At this temporal frequency, it can be difficult to fully capture distinct crop periods of initial inundation or harvest due to very active field management. Increased availability of Sentinel-1B, however, will enhance phenology monitoring. The rice phenology estimates are limited by the same satellite overpass dates. In general, our length of season estimates for season 1 seemed slightly lower than our local knowledge of about 100–115 days due to missing SAR data on June 28th (as some areas harvest around this time). However, it still highlights the utility of SAR for monitoring the length of season without the need to employ a complex algorithm or filtering.

We attribute relatively low single-rice producer's accuracy to the limited availability of training and validation data. This land cover class occupies less than 1% of the landscape and we could only obtain 41 polygons for validation. As such, when we adjusted the producer's accuracy to get unbiased areal estimates, the accuracy decreased significantly. For example, VH10m unadjusted producer's accuracy for single rice is 97.0% with only 5 pixels out of 166 confused with other classes. However, after calculating the accuracy using unbiased areal estimates, the accuracy decreases to 59%, whereas for double rice, the changes are less dramatic (i.e., just a few percentage points) due to appropriate sample size.

With further analysis, the results could be useful for land cover versus land use mapping. In addition, based on the SAR signal, it is possible to map single rice and double rice areas with only the first season of data. Results could be useful for aquaculture applications and land use planning. It may also be beneficial to integrate moderate resolution Sentinel-1 SAR imagery with high-resolution UAV-obtained imagery for relating to monitoring and improving crop growth parameter estimation [80].

VI. CONCLUSION

Using a random forest classifier, we compared single and double crop paddy rice mapping using six different datasets based on varied polarizations (VV, VH, and both) as well as different spatial resolutions (10 m and 20 m). Local incidence angles for the complete SAR time-series dataset suggest that imagery can be obtained for the whole year with negligible variation reducing the need to account for angular influence on backscatter. The time-series

Sentinel-1 SAR imagery was able to estimate start of season, end of season, and length of season for each rice crop at the commune level with promising results. Rice mapping estimates for the six datasets suggested the most accurate dataset to be VVVH10m (93.5% OA), whereas 20 m datasets generally had lower overall, user's and producer's accuracies compared to the 10 m datasets. Thematic change between the datasets suggested the least spatial variation in classes to be between VH and VVVH (10 and 20 m). The most common difference was between double crop rice and nonrice areas. About 20 m datasets overestimated rice land area more compared with 10 m datasets, as pixels were too large to capture small roads and ditches within paddy fields. The 20 m datasets, however, could be well representative of not only rice land cover, but especially rice land use. Province-level variation in mapped rice areas suggested the most occurring with VV20m, and also more variation in single rice than double rice based on the coefficient of variation. Moderately high spatial variation was found at the commune level with the maximum variation in rice area as 20% with VV10m and VH10m. This spatial variation could be critical for spatially explicit land cover mapping applications. AAD and CV results suggest communes in the northern portion of the study area and those immediately surrounding Hanoi City have the most proportional variation. This is important as these areas are subject to peri-urban expansion and important for air quality studies as areas closest to the city could have the highest impact on urban air quality.

Overall our study compared six different datasets (VV10m, VV20m, VH10m, VH20m, VVVH10m, and VVVH20m) for mapping paddy rice, evaluated importance of input bands from different dates for classification, estimated rice phenology, and calculated rice landscape metrics. The results from our study provide useful insights for crop mapping/monitoring efforts using SAR datasets in general and particularly within the Red River Delta of Vietnam.

ACKNOWLEDGMENT

The authors would like to thank T. N. T. Nguyen and H. Q. Bui (Vietnam National University Hanoi) for field assistance, and W. Salas and N. Torbick (Applied Geosolutions, LLC) for SAR expertise. K. Lasko would like to thank M. Campbell (Geospatial Research Lab) and S. Jantz (UMD) for support and also thanks his Ph.D. committee members including C. Justice, K. Vadrevu, I. Csiszar, L. Giglio, and M. Hansen for support. Authors would also thank the European Space Agency for the open data policy and Alaska Satellite Facility for hosting a mirror of the Sentinel-1 data.

REFERENCES

- [1]. General Statistics Office of Vietnam, "Agriculture, Forestry, and Trade," 2016 [Online]. Available: http://www.gso.gov.vn/Default_en.aspx?tabid=491
- [2]. Pham VC, Pham TTH, Tong THA, Nguyen TTH, and Pham NH, "The conversion of agricultural land in the peri-urban areas of Hanoi (Vietnam): patterns in space and time," *J. Land Use Sci.*, vol. 10, no. 2, pp. 224–242, 2015.
- [3]. Whitcraft AK, Vermote EF, Becker-Reshef I, and Justice CO, "Cloud cover throughout the agricultural growing season: Impacts on passive optical earth observations," *Remote Sens. Environ.*, vol. 156, pp. 438–447, 2015.
- [4]. Paudyal DR and Aschbacher J, "Land-cover separability studies of filtered ERS-1 SAR images in the tropics," in *Proc. Int. Geosci. Remote Sens. Symp. Better Understanding Earth Environ.*, 1993, 1216–1218.

- [5]. Aschbacher J, Pongsrihadulchai A, Karnchanasutham S, Rodprom C, Paudyal DR, and Le Toan T, "Assessment of ERS-1 SAR data for rice crop mapping and monitoring," in Proc. Int. Geosci. Remote Sens. Symp. Quantitative Remote Sens. Sci. Appl, 1995, vol. 3, pp. 2183–2185.
- [6]. Takeuchi S and Suwanwerakamton R, "Monitoring of land cover conditions in paddy fields using multitemporal SAR data," Int. Archives Photogramm. Remote Sens, vol. 31, pp. 683–688, 1996.
- [7]. Chakraborty M, Panigrahy ES, and Sharma SA, "Discrimination of rice crop grown under different cultural practices using temporal ERS-1 synthetic aperture radar data," ISPRS J. Photogramm. Remote Sens, vol. 52, no. 4, 183–191, 1997.
- [8]. Le Toan T et al., "Rice crop mapping and monitoring using ERS-1 data based on experiment and modeling results," IEEE Trans. Geosci. Remote Sens, vol. 35, no. 1, pp. 41–56, 1997.
- [9]. Liew SC, Kam SP, Tuong TP, Chen P, Minh VQ, and Lim H, "Application of multitemporal ERS-2 synthetic aperture radar in delineating rice cropping systems in the mekong river delta, Vietnam," IEEE Trans. Geosci. Remote Sens, vol. 36, no. 5, pp. 1412–1420, Sep. 1998.
- [10]. Yun S, Cuizhen W, Xiangtao F, and Hao L, "Estimation of rice growth status using RADARSAT data," IEEE Int. Geosci. Remote Sens. Remote Sensing-A Scientific Vision Sustain. Develop, vol. 3, pp. 1430–1432, Aug. 1997.
- [11]. Ribbes F, "Rice field mapping and monitoring with RADARSAT data," Int. J. Remote Sens, vol. 20, no. 4, pp. 745–765, 1999.
- [12]. Panigrahy S, Manjunath KR, Chakraborty M, Kundu N, and Parihar JS, "Evaluation of RADARSAT standard beam data for identification of potato and rice crops in India," ISPRS J. Photogramm. Remote Sens, vol. 54, no. 4, pp. 254–262, 1999.
- [13]. Shao Y et al., "Rice monitoring and production estimation using multitemporal RADARSAT," Remote Sens. Environ, vol. 76, no. 3, pp. 310–325, 2001.
- [14]. Lee KS and Lee SI, "Assessment of post-flooding conditions of rice fields with multi-temporal satellite SAR data," Int. J. Remote Sens, vol. 24, no. 17, pp. 3457–3465, 2003.
- [15]. Suga Y, Takeuchi S, Oguro Y, and Konishi T, "Monitoring of rice planted areas using space-borne SAR data," Int. Arch. Photogramm. Remote Sens, vol. 33, pp. 1480–1483, 2000.
- [16]. Inoue Y et al., "Season-long daily measurements of multifrequency (Ka, Ku, X, C, and L) and full-polarization backscatter signatures over paddy rice field and their relationship with biological variables," Remote Sens. Environ, vol. 81, no. 2, pp. 194–204, 2002.
- [17]. Chen C and McNairn H, "A neural network integrated approach for rice crop monitoring," Int. J. Remote Sens, vol. 27, no. 7, pp. 1367–1393, 2006.
- [18]. Salas W et al., "Mapping and modelling of greenhouse gas emissions from rice paddies with satellite radar observations and the DNDC biogeochemical model," Aquatic Conservation: Marine Freshwater Ecosyst, vol. 17, no. 3, pp. 319–329, 2007.
- [19]. Zhang Y, Wang C, Wu J, Qi J, and Salas WA, "Mapping paddy rice with multitemporal ALOS/PALSAR imagery in southeast China," Int. J. Remote Sens, vol. 30, no. 23, 6301–6315, 2009.
- [20]. Lam-Dao N, Apan A, Young FR, Le-Van T, Le-Toan T, and Bouvet A, "Rice monitoring using ENVISAT-ASAR data: Preliminary results of a case study in the Mekong River Delta, Vietnam," in Proc. 28th Asian Conf. Remote Sens, Nov. 2007, pp. 1–7.
- [21]. Bouvet A, Le Toan T, and Lam-Dao N, "Monitoring of the rice cropping system in the mekong delta using ENVISAT/ASAR dual polarization data," IEEE Trans. Geosci. Remote Sens, vol. 47, no. 2, pp. 517–526, Feb. 2009.
- [22]. Jia K, Li Q, Tian Y, Wu B, Zhang F, and Meng J, "Crop classification using multi-configuration SAR data in the north china plain," Int. J. Remote Sens, vol. 33, no. 1, pp. 170–183, 2012.
- [23]. Nguyen DB, Clauss K, Cao S, Naeimi V, Kuenzer C, and Wagner W, "Mapping rice seasonality in the Mekong Delta with multiyear Envisat ASAR WSM data," Remote Sens, vol. 7, no. 12, pp. 15868–15893, 2015.
- [24]. Pei Z, Zhang S, Guo L, McNairn H, Shang J, and Jiao X, "Rice identification and change detection using TerraSAR-X data," Can. J. Remote Sens, vol. 37, no. 1, pp. 151–156, 2011.
- [25]. Gebhardt S, Huth J, Nguyen LD, Roth A, and Kuenzer C, "A comparison of TerraSAR-X Quadpol backscattering with RapidEye multispectral vegetation indices over rice fields in the Mekong Delta, Vietnam," Int. J. Remote Sens, vol. 33, no. 24, pp. 7644–7661, 2012.

- [26]. Inoue Y, Sakaiya E, and Wang C, "Capability of C-band backscattering coefficients from high-resolution satellite SAR sensors to assess biophysical variables in paddy rice," *Remote Sens. Environ.*, vol. 140, pp. 257–266, 2014.
- [27]. Nelson A et al., "Towards an operational SAR-based rice monitoring system in Asia: Examples from 13 demonstration sites across Asia in the RIICE project," *Remote Sens.*, vol. 6, no. 11, pp. 10773–10812, 2014.
- [28]. Jiao X et al., "Object-oriented crop mapping and monitoring using multitemporal polarimetric RADARSAT-2 data," *ISPRS J. Photogramm. Remote Sens.*, vol. 96, pp. 38–46, 2014.
- [29]. Hoang HK, Bernier M, Duchesne S, and Tran YM, "Rice mapping using RADARSAT-2 dual-and quad-pol data in a complex land-use Watershed: Cau River Basin (Vietnam)," *IEEE J. Sel. Topics Appl. Earth Observ. Remote Sens.*, vol. 9, no. 7, pp. 3082–3096, Jul. 2016.
- [30]. Asilo S, de Bie K, Skidmore A, Nelson A, Barbieri M, and Maunahan A, "Complementarity of two rice mapping approaches: Characterizing strata mapped by hypertemporal MODIS and rice paddy identification using multitemporal SAR," *Remote Sens.*, vol. 6, no. 12, pp. 12789–12814, 2014.
- [31]. Karila K, Nevalainen O, Krooks A, Karjalainen M, and Kaasalainen S, "Monitoring changes in rice cultivated area from SAR and optical satellite images in Ben Tre and Tra Vinh Provinces in Mekong Delta, Vietnam," *Remote Sens.*, vol. 6, no. 5, pp. 4090–4108, 2014.
- [32]. Torbick N, Chowdhury D, Salas W, and Qi J, "Monitoring rice agriculture across myanmar using time series sentinel-1 assisted by Landsat-8 and PALSAR-2," *Remote. Sens.*, vol. 9, no. 2, p. 119, 2017.
- [33]. Nguyen DB, Gruber A, and Wagner W, "Mapping rice extent and cropping scheme in the Mekong Delta using Sentinel-1A data," *Remote Sens. Lett.*, vol. 7, no. 12, pp. 1209–1218, 2016.
- [34]. Mansaray LR, Zhang D, Zhou Z, and Huang J, "Evaluating the potential of temporal Sentinel-1A data for paddy rice discrimination at local scales," *Remote Sens. Lett.*, vol. 8, no. 10, pp. 967–976, 2017.
- [35]. Son NT, Chen CF, Chen CR, and Minh VQ, "Assessment of Sentinel-1A data for rice crop classification using random forests and support vector machines," *Geocarto Int.*, pp. 1–15, 2017.
- [36]. Steele-Dunne SC, McNairn H, Monsivais-Huertero A, Judge J, Liu PW, and Papatianassiou K, "Radar remote sensing of agricultural canopies: A review," *IEEE J. Sel. Topics Appl. Earth Observ. Remote Sens.*, vol. 10, no. 5, pp. 2249–2273, 5 2017.
- [37]. Whitcomb J, Moghaddam M, McDonald K, Kellndorfer J, and Podest E, "Mapping vegetated wetlands of Alaska using L-band radar satellite imagery," *Can. J. Remote Sens.*, vol. 35, no. 1, pp. 54–72, 2009.
- [38]. White L, Brisco B, Dabboor M, Schmitt A, and Pratt A, "A collection of SAR methodologies for monitoring wetlands," *Remote Sens.*, vol. 7, no. 6, pp. 7615–7645, 2015.
- [39]. Wang W et al., "A fully polarimetric SAR imagery classification scheme for mud and sand flats in intertidal zones," *IEEE Trans. Geosci. Remote Sens.*, vol. 55, no. 3, pp. 1734–1742, Mar. 2017.
- [40]. Shiraishi T, Motohka T, Thapa RB, Watanabe M, and Shimada M, "Comparative assessment of supervised classifiers for land use–land cover classification in a tropical region using time-series PALSAR mosaic data," *IEEE J. Sel. Topics Appl. Earth Observ. Remote Sens.*, vol. 7, no. 4, pp. 1186–1199, Apr. 2014.
- [41]. Torbick N, Salas W, Chowdhury D, Ingraham P, and Trinh M, "Mapping rice greenhouse gas emissions in the Red River Delta, Vietnam," *Carbon Manag.*, vol. 8, no. 1, pp. 99–108, 2017.
- [42]. Waske B and Braun M, "Classifier ensembles for land cover mapping using multitemporal SAR imagery," *ISPRS J. Photogramm. Remote Sens.*, vol. 64, no. 5, pp. 450–457, 2009.
- [43]. Sonobe R, Tani H, Wang X, Kobayashi N, and Shimamura H, "Random forest classification of crop type using multi-temporal TerraSAR-X dual-polarimetric data," *Remote Sens. Lett.*, vol. 5, no. 2, pp. 157–164, 2014.
- [44]. Zhang H et al., "Object-based crop classification using multi-temporal SPOT-5 imagery and textural features with a random forest classifier," *Geocarto Int.*, pp. 1–40, 2017.
- [45]. Uhlmann S and Kiranyaz S, "Integrating color features in polarimetric SAR image classification," *IEEE Trans. Geosci. Remote Sens.*, vol. 52, no. 4, pp. 2197–2216, Apr. 2014.

- [46]. Lopez-Sanchez JM, Cloude SR, and Ballester-Berman JD, "Rice phenology monitoring by means of SAR polarimetry at X-band," *IEEE Trans. Geosci. Remote Sens.*, vol. 50, no. 7, pp. 2695–2709, Jul. 2012.
- [47]. Jiao X et al., "Object-oriented crop mapping and monitoring using multitemporal polarimetric RADARSAT-2 data," *ISPRS J. Photogramm. Remote Sens.*, vol. 96, pp. 38–46, 2014.
- [48]. Koppe W et al., "Rice monitoring with multi-temporal and dual polarimetric TerraSAR-X data," *Int. J. Appl. Earth Observ. Geoinf.*, vol. 21, pp. 568–576, 2013.
- [49]. Erten E, Rossi C, Yuzugullu O, and Hajnsek I, "Phenological growth" stages of paddy rice according to the BBCH scale and SAR images," in *Proc. IEEE Int. Geosci. Remote Sens. Symp.*, Jul. 2014, pp. 1017–1020.
- [50]. Erten E, Rossi C, and Yuzugullu O, "Polarization impact in TanDEM-X" data over vertical-oriented vegetation: The paddy-rice case study," *IEEE Geosci. Remote Sens. Lett.*, vol. 12, no. 7, pp. 1501–1505, Jul. 2015.
- [51]. Lopez-Sanchez JM, Vicente-Guijalba F, Ballester-Berman JD, and Cloude SR, "Polarimetric response of rice fields at C-band: Analysis and phenology retrieval," *IEEE Trans. Geosci. Remote Sens.*, vol. 52, no. 5, pp. 2977–2993, 5 2014.
- [52]. Kucuk C, Taskin G, and Erten E, "Paddy-rice phenology classification based on machine-learning methods using multitemporal co-polar X-band SAR images," *IEEE J. Sel. Topics Appl. Earth Observ. Remote Sens.*, vol. 9, no. 6, pp. 2509–2519, Jun. 2016.
- [53]. de Bernardis CG, Vicente-Guijalba F, Martinez-Marin T, and Lopez-Sanchez JM, "Estimation of key dates and stages in rice crops using dual-polarization SAR time series and a particle filtering approach," *IEEE J. Sel. Topics Appl. Earth Observ. Remote Sens.*, vol. 8, no. 3, pp. 1008–1018, Mar. 2015.
- [54]. Xie L, Zhang H, Wu F, Wang C, and Zhang B, "Capability of rice mapping using hybrid polarimetric SAR data," *IEEE J. Sel. Topics Appl. Earth Observ. Remote Sens.*, vol. 8, no. 8, pp. 3812–3822, Aug. 2015.
- [55]. Yuzugullu O, Erten E, and Hajnsek I, "Rice growth monitoring by means of X-band co-polar SAR: Feature clustering and BBCH scale," *IEEE Geosci. Remote Sens. Lett.*, vol. 12, no. 6, pp. 1218–1222, Jun. 2015.
- [56]. Oyoshi K, Tomiyama N, Okumura T, Sobue S, and Sato J, "Mapping rice-planted areas using time-series synthetic aperture radar data for the Asia-RiCE activity," *Paddy Water Environ.*, vol. 14, no. 4, pp. 463–472, Oct. 2016.
- [57]. Whitcraft AK, Becker-Reshef I, and Justice CO, "A framework for defining spatially explicit earth observation requirements for a global agricultural monitoring initiative (GEOGLAM)," *Remote Sens.*, vol. 7, no. 2, pp. 1461–1481, 2015.
- [58]. Lasko K et al., "Satellites may underestimate rice residue and associated burning emissions in Vietnam," *Environ. Res. Lett.*, vol. 12, no. 8, 2017, Art. no. 085006.
- [59]. Xiao X et al., "Mapping paddy rice agriculture in southern China using multi-temporal MODIS images," *Remote Sens. Environ.*, vol. 95, no. 4, pp. 480–492, 2005.
- [60]. Kontgis C, Schneider A, and Ozdogan M, "Mapping rice paddy extent and intensification in the vietnamese mekong river delta with dense time stacks of landsat data," *Remote Sens. Environ.*, vol. 169, pp. 255–269, 2015.
- [61]. Duong PT and Yoshiro H, "Current Situation and Possibilities of Rice Straw Management in Vietnam," 2015 [Online]. Available: http://www.jsrsai.jp/Annual_Meeting/PROG_52/Resume/C02-4.pdf
- [62]. Dey MM and Ahmed M, "Aquaculture—food and livelihoods for the poor in Asia: A brief overview of the issues," *Aquaculture Econ. Manag.*, vol. 9, no. 1/2, pp. 1–10, 2005.
- [63]. Ottinger M, Clauss K, and Kuenzer C, "Large-scale assessment of coastal aquaculture ponds with sentinel-1 time series data," *Remote Sens.*, vol. 9, no. 5, p. 440, 2017.
- [64]. Zuhlke M et al., "SNAP (sentinel application platform) and the ESA sentinel 3 toolbox," *Sentinel-3 Sci. Workshop.*, vol. 734, p. 21, Dec. 2015.
- [65]. Breiman L, "Random forests," *Mach. Learn.*, vol. 45, no. 1, pp. 5–32, 2001.
- [66]. Congalton RG and Green K, *Assessing the Accuracy of Remotely Sensed Data: Principles and Practices* Boca Raton, FL, USA: CRC Press, 2008.

- [67]. Olofsson P, Foody GM, Herold M, Stehman SV, Woodcock CE, and Wulder MA, "Good practices for estimating area and assessing accuracy of land change," *Remote Sens. Environ*, vol. 148, pp. 42–57, 2014.
- [68]. Fukunaga K and Hostetler L, "The estimation of the gradient of a density function, with applications in pattern recognition," *IEEE Trans. Inf. Theory*, vol. 21, no. 1, pp. 32–40, Jan. 1975.
- [69]. Comaniciu D and Meer P, "Mean shift: A robust approach toward feature space analysis," *IEEE Trans. Pattern Anal. Mach. Intell*, vol. 24, no. 5, pp. 603–619, 5 2002.
- [70]. Su T and Zhang S, "Local and global evaluation for remote sensing image segmentation," *ISPRS J. Photogramm. Remote Sens*, vol. 130, pp. 256–276, Aug. 2017.
- [71]. Senthilnath J, Omkar SN, Mani V, Tejovanth N, Diwakar PG, and Shenoy AB, "Hierarchical clustering algorithm for land cover mapping using satellite images," *IEEE J. Sel. Topics Appl. Earth Observ. Remote Sens*, vol. 5, no. 3, pp. 762–768, Jun. 2012.
- [72]. Choudhury I and Chakraborty M, "SAR signature investigation of rice crop using RADARSAT data," *Int. J. Remote Sens*, vol. 27, no. 3, pp. 519–534, 2006.
- [73]. Chen CF, Son NT, Chen CR, Chang LY, and Chiang SH, "Rice crop mapping using Sentinel-1A phonological metrics," *ISPRS-Int. Archives Photogramm*, Vol. XLI-B8, pp. 863–865, 2016.
- [74]. Nguyen D, Wagner W, Naeimi V, and Cao S, "Rice-planted area extraction by time series analysis of ENVISAT ASAR WS data using a phenology-based classification approach: A case study for Red River Delta, Vietnam," *Int. Archives Photogramm., Remote Sens. Spatial Inf. Sci*, vol. 40, no. 7, p. 77, 2015.
- [75]. Hoang KH, Bernier M, Duchesne S, and Tran MY, "Classification of rice fields in a complex land-use watershed in Northern Vietnam using RADARSAT-2 data," in *Proc. IEEE Int. Geosci. Remote Sens. Symp*, Jul. 2014, pp. 1501–1503.
- [76]. Boschetti M et al., "Rapid assessment of crop status: An application of MODIS and SAR data to rice areas in Leyte, Philippines affected by Typhoon Haiyan," *Remote Sens*, vol. 7, no. 6, pp. 6535–6557, 2015.
- [77]. Belgiu M and Dragut L, "Random forest in remote sensing: A review of applications and future directions," *ISPRS J. Photogramm. Remote Sens*, vol. 114, pp. 24–31, 2016.
- [78]. Loosvelt L, Peters J, Skriver H, De Baets B, and Verhoest NE, "Impact of reducing polarimetric SAR input on the uncertainty of crop classifications based on the random forests algorithm," *IEEE Trans. Geosci. Remote Sens*, vol. 50, no. 10, pp. 4185–4200, Oct. 2012.
- [79]. Rodriguez-Galiano VF, Chica-Olmo M, Abarca-Hernandez F, Atkinson PM, and Jeganathan C, "Random Forest classification of Mediterranean land cover using multi-seasonal imagery and multi-seasonal texture," *Remote Sens. Environ*, vol. 121, pp. 93–107, 2012.
- [80]. Uto K, Seki H, Saito G, and Kosugi Y, "Characterization of rice paddies by a UAV-mounted miniature hyperspectral sensor system," *IEEE J. Sel. Topics Appl. Earth Observ. Remote Sens*, vol. 6, no. 2, pp. 851–860, Apr. 2013.

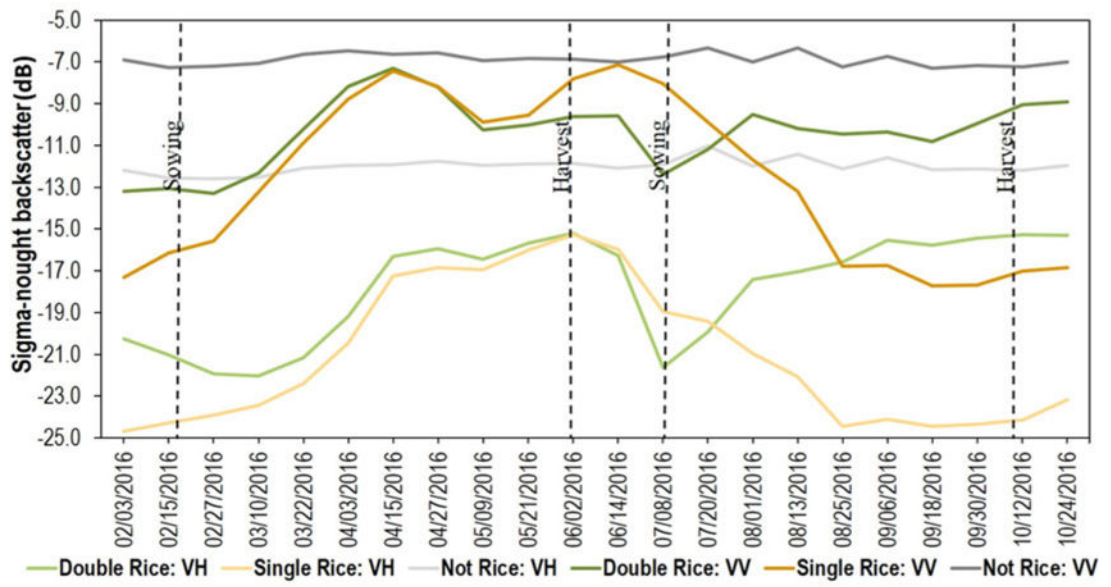


Fig. 1. Time-series SAR signal over different land cover types and polarizations in the study area.

NASA Author Manuscript

NASA Author Manuscript

NASA Author Manuscript

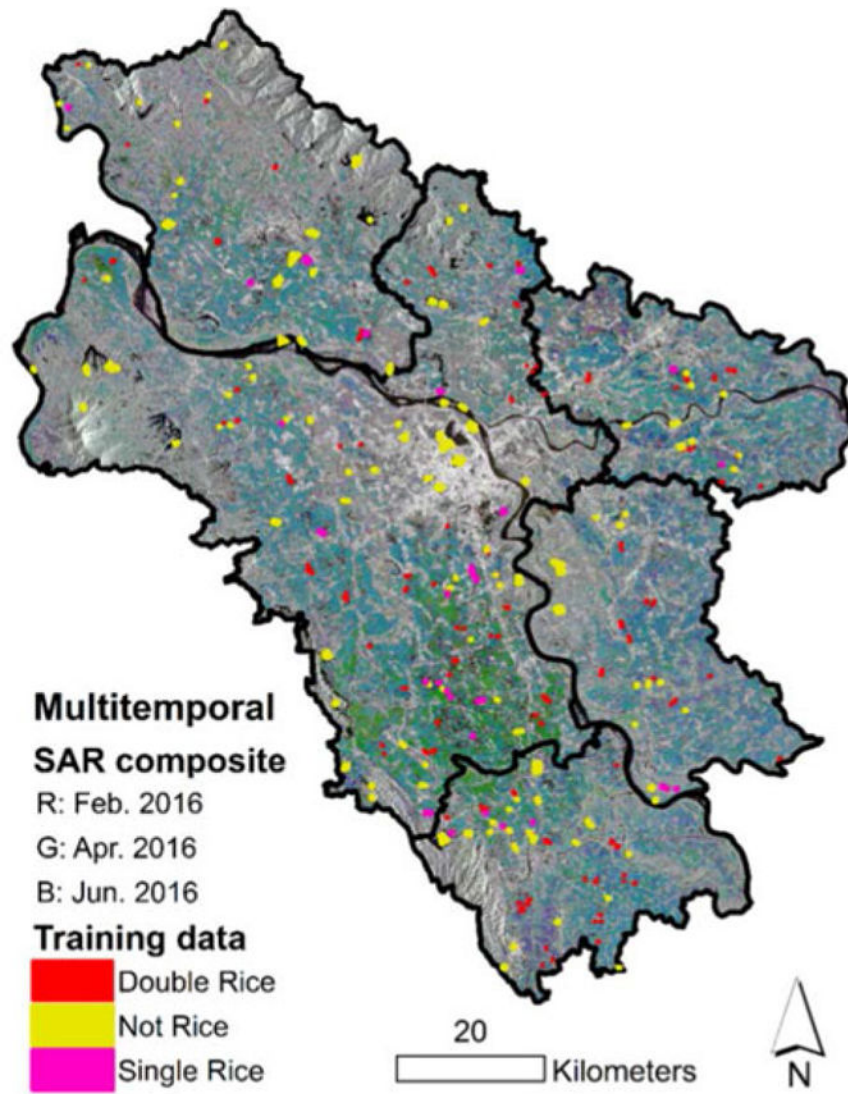


Fig. 2. Multitemporal SAR composite with training polygons overlaid. Note: border thickness of training data exaggerated for visualization.

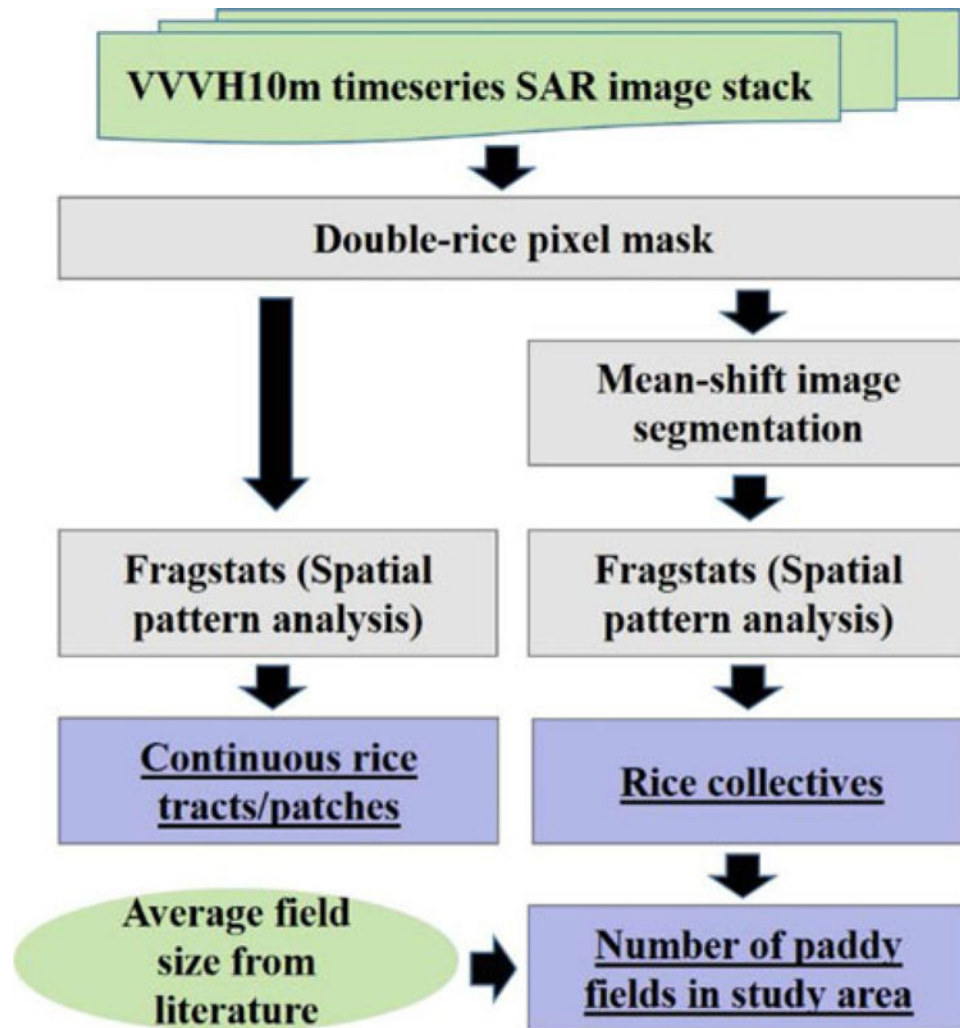


Fig. 3. Landscape analysis flowchart. Landscape-scale analysis using Fragstats and mean-shift image segmentation were used to derive: 1) continuous rice tracts/patches, 2) size and number of rice collectives; 3) the total number of paddy rice fields.

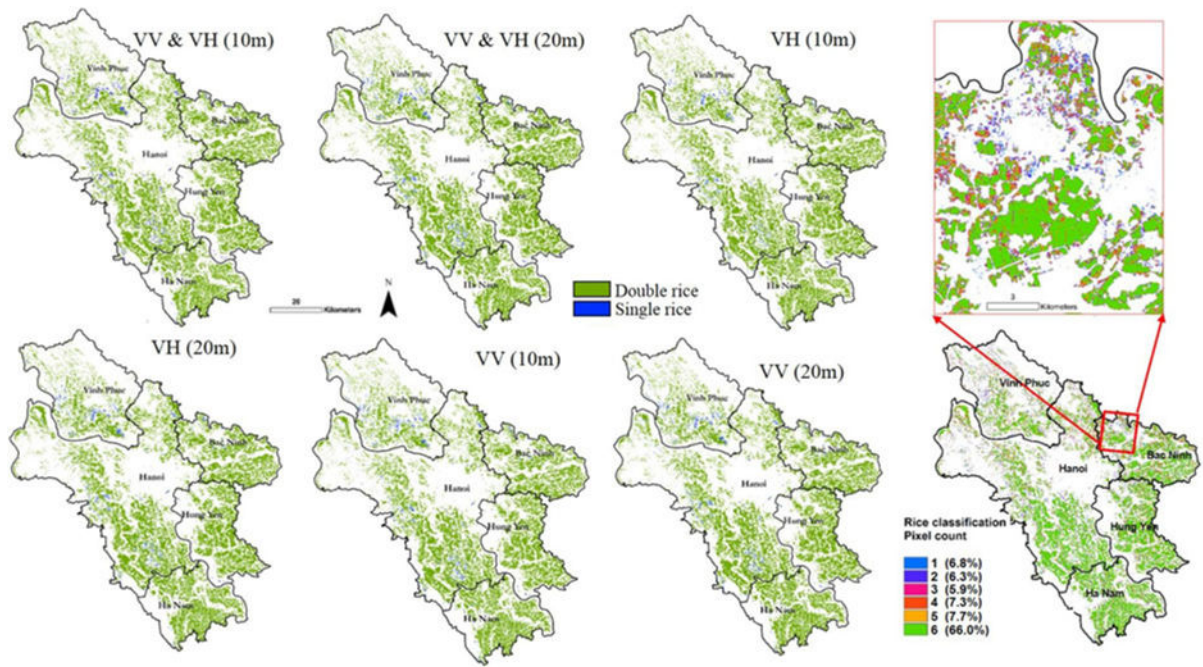


Fig. 4. Paddy rice maps for each dataset and a pixel count of double-rice agreement between the six datasets on the right side.

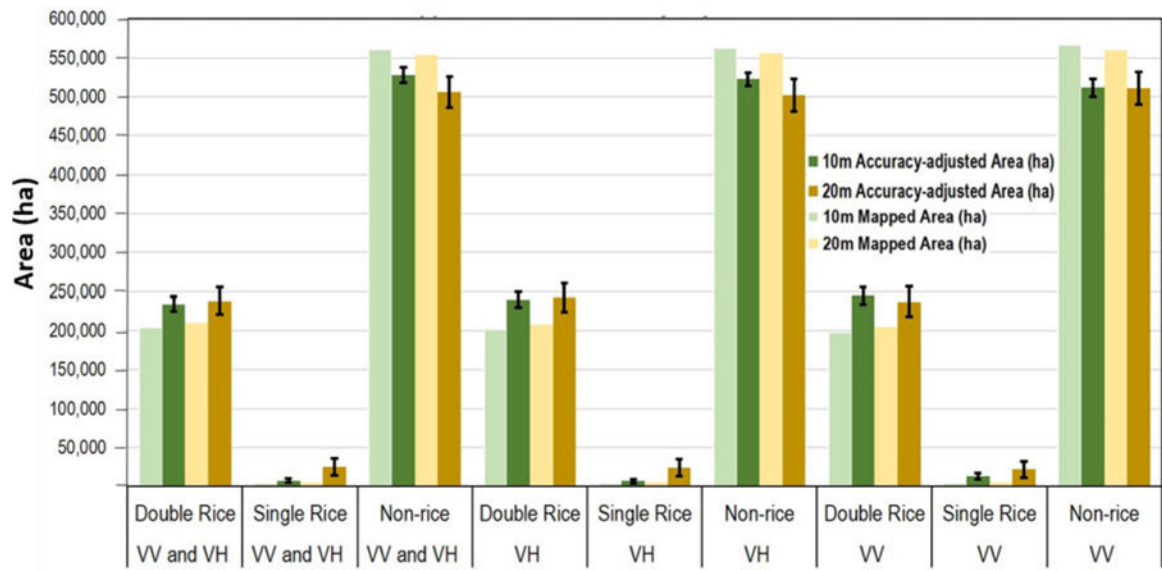


Fig. 5. Mapped areas and accuracy-adjusted areas.

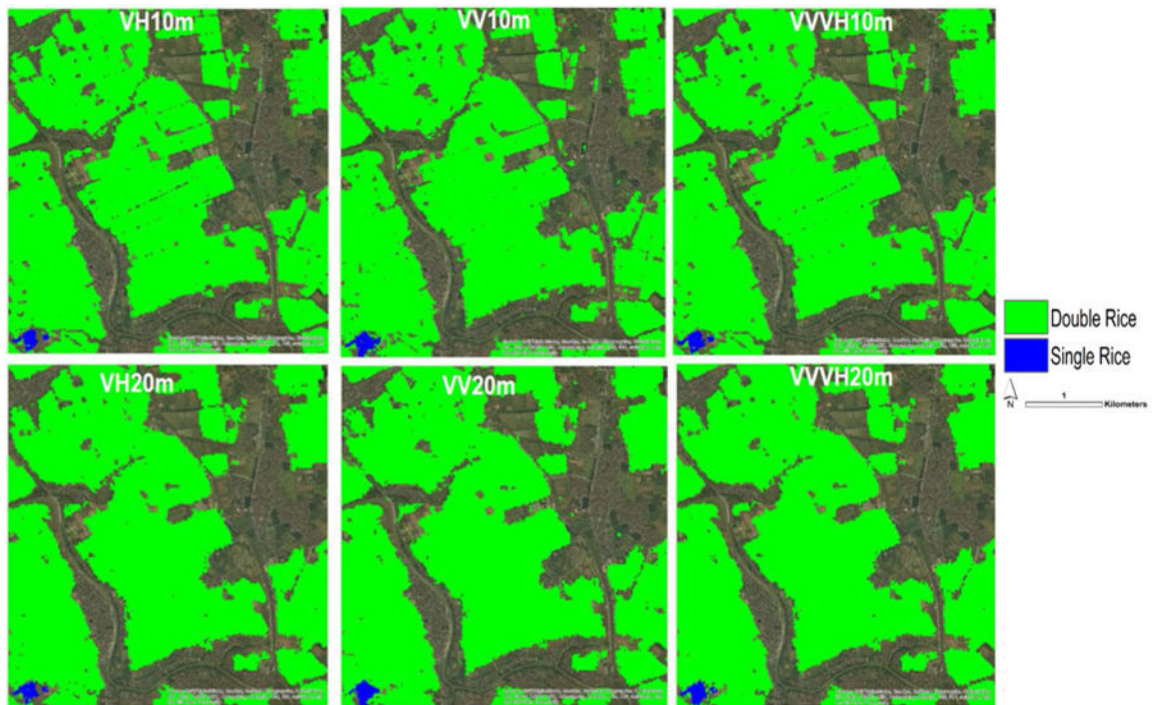


Fig. 6.
Rice areal variation zoomed to Hanoi province highlighting variation in each dataset.



Fig. 7. Province-level rice variation. Double rice and single crop rice province-level z-scores indicating deviation from the mean.

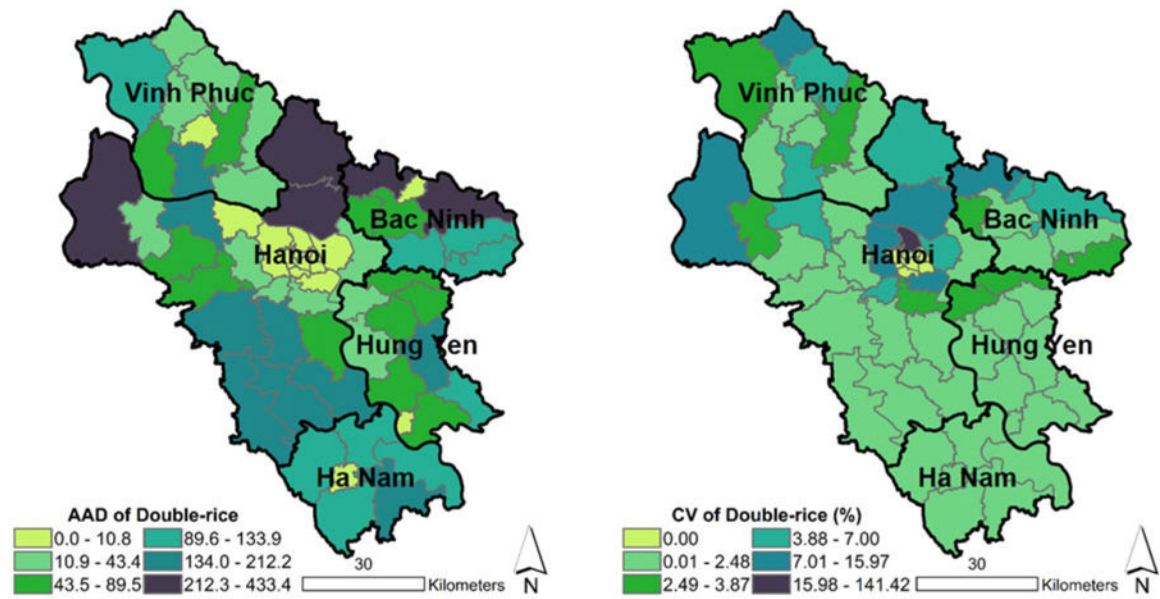


Fig. 8. Commune-level rice variation. AAD and CV for double rice area per commune with province boundaries overlaid. Results suggest most AAD in communes with high rice mapped areas, while CV results suggest communes in the north tended to have higher percentage variation likely attributed to mapped area difficulties in more mosaicked landscapes with smaller fields.

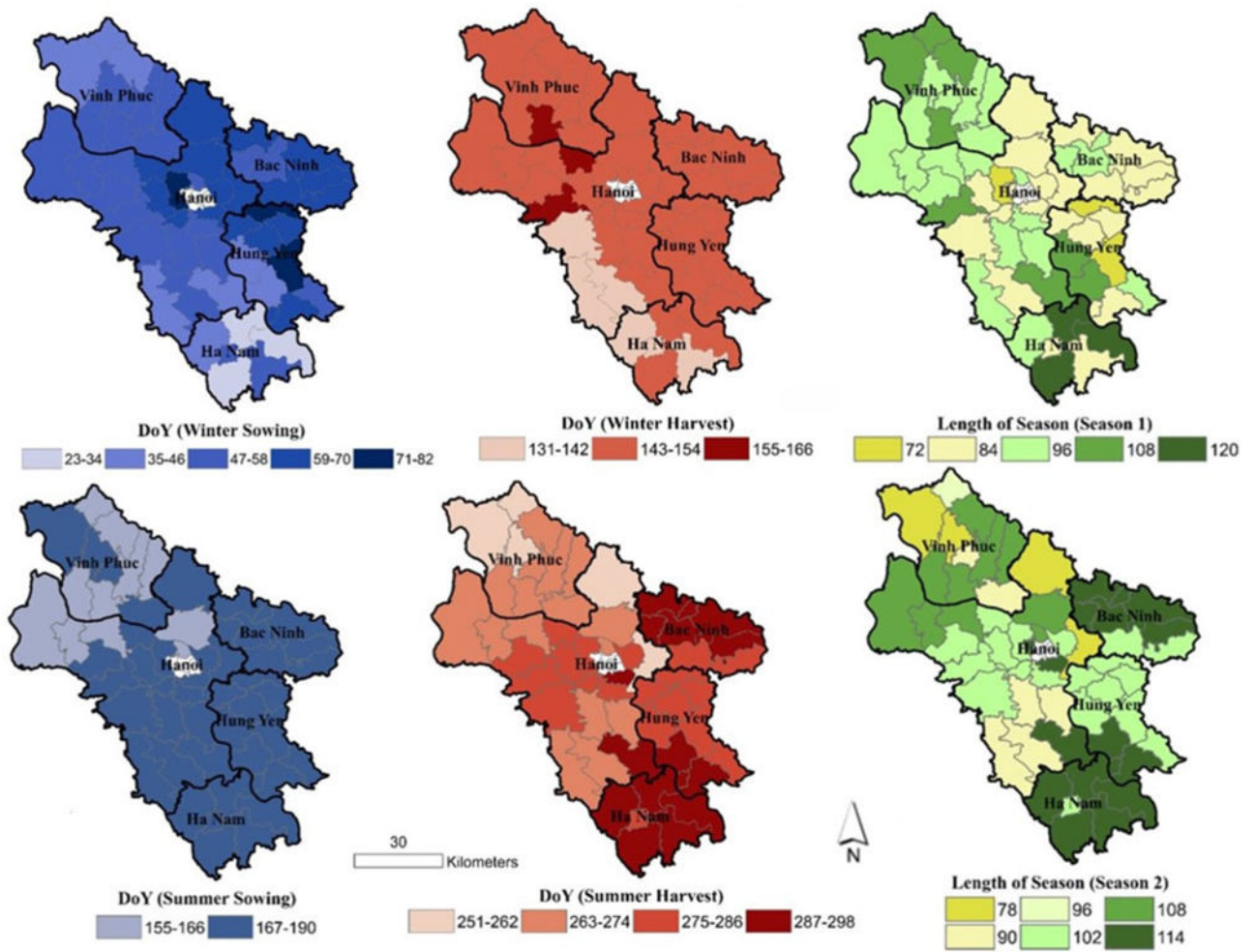


Fig. 9. Commune-level rice phenology. Commune-level sowing and harvest day of year (DoY) ranges based on Sentinel-1 signal. Reason for minimal variation in summer sowing is due to missing data for ~06/28/2016, thus actual range is bigger.

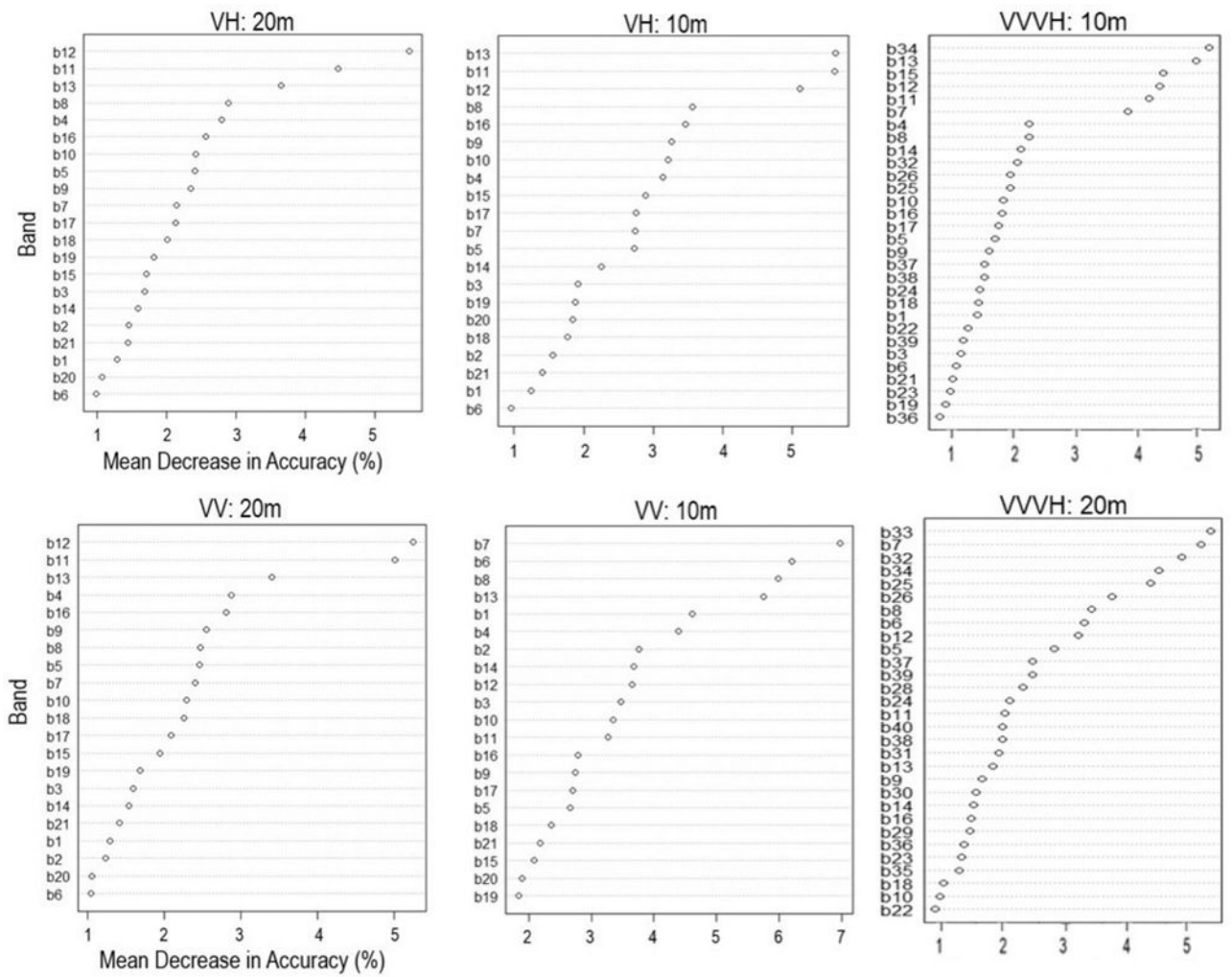


Fig. 10. Mean decrease in out of bag accuracy (%): suggests bands from all parts of rice stage (planting/growth/harvest) are important, with bands from second season planting and first season harvest generally most critical. Note for VVVH graphs, bands 1–22 are VV and bands 23–44 are VH.

TABLE I

SAR INCIDENCE ANGLE VARIATION ($^{\circ}$)

Band	Date	Avg Angle (Double Rice)	Std Angle (Double Rice)	Avg angle (Single Rice)	Std Angle (Single Rice)	Avg angle (Not Rice)	Std Angle (Not Rice)
1	02/03/2016	38.630	3.343	39.304	3.328	39.547	6.414
2	02/15/2016	38.639	3.347	39.314	3.326	39.547	6.414
3	02/27/2016	38.640	3.349	39.316	3.327	39.543	6.414
4	03/10/2016	38.629	3.341	39.306	3.328	39.550	6.412
5	03/22/2016	38.640	3.350	39.326	3.322	39.539	6.411
6	04/03/2016	38.644	3.351	39.334	3.326	39.538	6.409
7	04/15/2016	38.640	3.343	39.325	3.322	39.545	6.411
8	04/27/2016	38.644	3.345	39.327	3.322	39.546	6.411
9	05/09/2016	38.637	3.344	39.322	3.325	39.543	6.410
10	05/21/2016	38.644	3.353	39.331	3.337	39.542	6.408
11	06/02/2016	38.624	3.337	39.306	3.327	39.547	6.412
12	06/14/2016	38.634	3.342	39.315	3.325	39.546	6.412
13	07/08/2016	38.632	3.347	39.303	3.327	39.547	6.410
14	07/20/2016	38.632	3.340	39.313	3.326	39.548	6.412
15	08/01/2016	38.620	3.336	39.302	3.327	39.547	6.412
16	08/13/2016	38.627	3.339	39.303	3.327	39.550	6.411
17	08/25/2016	38.627	3.339	39.304	3.327	39.550	6.412
18	09/06/2016	38.626	3.336	39.307	3.327	39.553	6.412
19	09/18/2016	38.629	3.340	39.307	3.327	39.548	6.412
20	09/30/2016	38.629	3.340	39.310	3.325	39.543	6.412
21	10/12/2016	38.638	3.346	39.325	3.327	39.542	6.410
22	10/24/2016	38.640	3.344	39.325	3.322	39.543	6.411

Local incidence angle, θ , variation in SAR imagery per mapped land cover class for VV&VH 10 m dataset: Minimal variation through time in all categories. "Not rice" areas have higher standard deviation due to mountainous areas.

TABLE II

DATASET DESCRIPTIONS

Dataset name	Description
VV10m	Vertical–vertical (VV) polarized bands at 10-m spatial resolution
VH10m	Vertical–horizontal (VH) polarized bands at 10-m spatial resolution
VVVH10m	Both VV and VH bands at 10-m resolution
VV20m	VV bands at 20-m spatial resolution
VH20m	VH bands at 20-m spatial resolution
VVVH20m	Both VV and VH bands at 20-m spatial resolution

NASA Author Manuscript

NASA Author Manuscript

NASA Author Manuscript

TABLE III

(A), (B) CONFUSION MATRICES

REFERENCE							REFERENCE						
VV and VH Class	Double rice	Single rice	Non-rice	Total	Adj. User's Acc.	Area (ha)	VV and VH Class	Double rice	Single rice	Non-rice	Total	Adj. User's Acc.	Mapped Area (ha)
Double rice	420	2	17	439	95.7% (0.09%)	214,565	Double rice	120	1	6	127	94.5% (0.35%)	220,356
Single rice	0	160	1	161	99.4% (0.10%)	4,719	Single rice	1	48	1	50	95.2% (1.02%)	5,533
Non-rice	68	4	916	988	92.7% (0.05%)	588,449	Non-rice	24	3	299	326	89.5% (0.18%)	581,839
Total	488	166	934	1588		807,733	Total	145	52	306	503		807,729
Adj. Producer's Acc.	83.5% (0.15%)	58.3% (0.59%)	98.5% (0.03%)				Adj. Producer's Acc.	82.9% (0.51%)	42.8% (1.90%)	98.1% (0.09%)			
Overall Accuracy: 93.5% (1.33%)							Overall Accuracy: 92.5% (2.52%)						
REFERENCE							REFERENCE						
VH Class	Double rice	Single rice	Non-rice	Total	Adj. User's Acc. (C.I)	Area (ha)	VH Class	Double rice	Single rice	Non-rice	Total	Adj. User's Acc.	Mapped Area (ha)
Double rice	410	0	13	423	96.9% (0.08%)	212,465	Double rice	117	0	7	124	94.4% (0.37%)	218,788
Single rice	0	161	3	164	98.2% (0.16%)	4,319	Single rice	0	48	1	49	98.0% (0.58%)	5,227
Non-rice	78	5	918	1001	91.7% (0.05%)	590,950	Non-rice	28	4	298	330	90.3% (0.18%)	583,713
Total	488	166	934	1588		807,733	Total	145	52	306	503		807,729
Adj. Producer's Acc	81.7% (0.16%)	59.0% (0.58%)	98.8% (0.02%)				Adj. Producer's Acc.	80.7% (0.54%)	42.0% (1.90%)	97.7% (0.10%)			
Overall Accuracy: 93.1% (1.38%)							Overall Accuracy: 91.4% (2.68%)						
REFERENCE							REFERENCE						
VV Class	Double rice	Single rice	Non-rice	Total	Adj. User's Acc. (C.I)	Area (ha)	VV Class	Double rice	Single rice	Non-rice	Total	Adj. User's Acc.	Mapped Area (ha)
Double rice	389	3	14	406	95.8% (0.10%)	208,276	Double rice	116	2	8	126	92.1% (0.42%)	214,903
Single rice	0	145	1	146	99.3% (0.11%)	4,908	Single rice	0	48	0	48	100% (0.00%)	5,450
Non-rice	99	13	919	1031	89.1% (0.06%)	594,549	Non-rice	29	2	298	329	90.6% (0.17%)	587,376
Total	488	161	934	1583		807,733	Total	145	52	306	503		807,729
Adj. Producer's Acc	77.8% (0.17%)	35.0% (0.58%)	98.7% (0.02%)				Adj. Producer's Acc.	79.3% (0.55%)	43.8% (1.91%)	97.5% (0.10%)			
Overall Accuracy: 90.9% (1.57%)							Overall Accuracy: 91.0% (2.75%)						

confusion matrices with associated pixels per class, mapped class area, and adjusted accuracies with confidence intervals based on calculated unbiased areal estimates for a) 10m data; and b) 20m data.

NASA Author Manuscript

NASA Author Manuscript

NASA Author Manuscript